Available online at www.sciencedirect.com

SciVerse ScienceDirect

Ceramics International 39 (2013) 2275–2281

CERAMICS INTERNATIONAL

www.elsevier.com/locate/ceramint

Designing the morphology of ceria particles by precursor complexes

S.J. Shih*, J.P. Huang

Department of Materials Science and Engineering, National Taiwan University of Science and Technology, 43, Sector 4, Keelung Road, Taipei 10607, Taiwan

Received 24 July 2012; received in revised form 25 August 2012; accepted 25 August 2012
Available online 1 September 2012

Abstract

Ceria-based materials are widely used as catalysts, catalyst supports and electrolytes in many industrial applications. The morphological requirements of ceria particles vary depending on their applications. Here we show that complex morphologies of ceria particles can be achieved by using precursor complexes in the spray pyrolysis (SP) method. Three precursor complexes have been investigated: the complex of cerium acetate hydrate (CeA) and cerium nitrate hydrate (CeN); CeA and cerium ammonium nitrate (CeAN); and CeN and CeAN. Our results suggest that the morphological formation mechanism is highly correlated with the factors of precursor solubilities, solvent evaporation rates and precursor melting temperatures.

Keywords: A. Powders: chemical preparation; B. Microstructure—final; B. Electron microscopy; D. CeO_2

1. Introduction

Ceria is known for industrial materials because of its superior properties of ion conductivity [1], thermal stability [2] and oxygen storage capacity [3], leading to the widespread use of ceria-based particles as components in applications such as solid oxide fuel cell (SOFC) electrolytes [1], catalyst supports [4] and carbon monoxide (CO) reduction catalysts [3]. In order to achieve optimal performance, the morphology requirements of ceria particles vary depending on their applications [1,3,4]. For example, SOFC electrolytes must be dense, and therefore solid ceria particles with minimum porosity are desirable [1]. For catalyst support applications, ceria particles with a porous structure provides greater, therefore leading to higher reaction efficiency [4]. When used as catalysts for CO oxidation, the hollow ceria structures offer the advantages of providing greater gas adsorption [3]. Furthermore, Du et al. [5] have recently reported that rod-shaped ceria particles with a high proportion of (100) and (110) surfaces are catalytically more active compared to spherical ceria particles with a high proportion of (111) surfaces. In addition, those authors also found that the ceria rods have higher ratio of Ce^{3+} (10.8%) compared to that (6.9%) of the spherical ceria particles. These examples illustrate that the morphology plays a significant role in governing the useful properties of ceria particles.

A number of methods have been used to synthesize ceria particles, including the sol–gel method [6,7], micro-emulsion [8], precipitation [9,10] and spray pyrolysis (SP) [11–15]. Here we have chosen the SP process because of its simple operation, continuous processing, production of high purity powder and chemistry flexibility [16]. Table 1 summarizes the previous reports of the four particle morphologies of solid, hollow, concaved and multiporous particles and their corresponding precursor solution (salt and solvent) used in the synthesis [11–15]. These reports establish that there is a strong correlation between particle morphology and the single salt precursor [11–15]. However, studies using precursor complexes are (multiple salt systems) are scarce. In order to obtain more complex morphologies for a wider range of industrial applications, it is important to develop the SP methods and the relevant formation mechanisms using precursor complexes.

In this study, three precursor complexes were applied to produce various morphologies, namely a mixture of cerium acetate hydrate (CeA) and cerium nitrate hydrate (CeN), a mixture of CeA and cerium ammonium nitrate (CeAN)

*Corresponding author. Tel.: +886 2 2730 3716; fax: +886 2 2737 6544.
E-mail address: shao-ju.shih@mail.ntust.edu.tw (S.-J. Shih).

0272-8842/$ - see front matter
http://dx.doi.org/10.1016/j.ceramint.2012.08.074

Table 1
Previous experimental results of various morphological ceria particles synthesized by SP.

Morphology	Salt	Solution	Particle size, (nm)	References
Solid	$(NH_4)_2Ce(NO_3)_6$	DI water	~30 to 600	Shih et al. [11]
Hollow	$Ce(NO_3)_3 \cdot 6H_2O$	DI water	~70 to 750	Kang et al. [12]
Hollow	$Ce(C_2H_3O_2)_3 \cdot 1.5H_2O$	DI water	~100 to 300	Shih et al. [13]
Concaved	$Ce(C_2H_3O_2)_3 \cdot 1.5H_2O$	DI water	~350 to 780	Chen et al. [14]
Multiporous	$Ce(NO_3)_3 \cdot 6H_2O$	DI water	~30 to 900	Shih et al. [15]

and a mixture of CeN and CeAN. The decomposition behaviors of the three salts were examined by the thermogravimetric analysis (TGA) and differential thermal analysis (DTA). The geometries and the crystallographic structures of the ceria particles were examined by transmission electron microscopy (TEM) and selected area electron diffraction (SAED). Also, the surface morphologies and surface areas of the particles were analyzed by scanning electron microscopy (SEM) and nitrogen adsorption and desorption isotherms (BET method), respectively. Our result shows that the different complex precursors lead to new complex morphologies of ceria particles via different SP formation mechanisms.

2. Experimental procedures

The ceria powders from the precursor complexes, including (i) 50 mol% CeA ($Ce(C_2H_3O_2)_3 \cdot 1.5H_2O$, 99.9%, Alfa Aesar, Johnson Matthey Co.) and 50 mol% CeN ($Ce(NO_3)_3 \cdot 6H_2O$, 99.5%, Alfa Aesar, Johnson Matthey Co.) (CeA+CeN), (ii) 50 mol% CeA and 50 mol% CeAN ($(NH_4)_2Ce(NO_3)_6$, 99.5%, Alfa Aesar, Johnson Matthey Co.) (CeA+CeAN) and (iii) 50 mol% CeN and 50 mol% CeAN (CeN+CeAN), were prepared using a laboratory-scale SP electrostatic deposition system. Initially, three cerium precursors were dissolved separately in de-ionized water to form three precursor solutions (1 wt%). In the SP process the precursor solution was first atomized into small droplets while an air flow with a controlled flow rate carried the droplets into the heated tubular reactor with three heating zones of 250, 650 and 350 °C. In the reactor the droplets undergo solvent evaporation, solute precipitation and precursor decomposition to convert into oxide particles. The resulting particles were then collected by a cylindrical electrostatic collector with an applied high-voltage potential of −16 kV.

The three salts of CeA, CeN and CeAN were characterized by the thermal analyses of TGA and DTA (TG–DTA 8120, Rigaku, USA) under an ambient airflow to remove decomposition products. The heating rate was 10 °C/min.

TEM specimens of the ceria particles from the precursors complexes of CeA+CeN, CeA+CeAN and CeN+CeAN were prepared by dispersing the particles in acetone using an ultrasonic bath for around 5 min, and then depositing a drop of suspension onto holey carbon film grids. The solvent on the carbon grids was evaporated at room temperature. The field emission gun-transmission electron microscope (Tecnai G2 F20, FEI, USA), operated at 200 keV, was used to examine the morphology and the crystallographic structure of the ceria powders. The morphologies of three ceria powders were obtained from numerous TEM micrographs, and more than 150 particles were examined to obtain the particle diameter distributions. The crystallographic structures of three particles are characterized by SAED from random selected particles with an aperture size of 800 nm.

Since projection images from TEM only reveal two-dimensional morphologies [13], surface morphologies were taken using field-emission scanning electron microscopy (FESEM, JSM-6500F, JEOL, Japan) to compare with the TEM images for three-dimensional morphologies.

The specific surface areas of the ceria powders were measured using the BET method (ASAP 2010, Micromeritics, USA) from nitrogen adsorption and desorption isotherm data obtained at −196 °C on a constant-volume adsorption apparatus. The as-prepared samples were degassed at 150 °C for 3 h before measurements. The average values and standard deviations of the specific surface areas from three repeated measurements were obtained.

3. Results and discussion

Fig. 1 shows the TGA and DTA analyses for the single salt systems of CeA, CeN and CeAN. Firstly, the four weight-loss stages for CeA (Fig. 1(a), obtained from TGA data with the temperature ranges of ~50 to ~110 °C, ~110 to ~160 °C, ~160 to ~280 °C and ~280 to ~800 °C are attributed to formation of $Ce(C_2H_3O_2)_3 \cdot H_2O$ (97% of CeA), $Ce(C_2H_3O_2)_3$ (92% of CeA), $Ce_2O_2CO_3$ (64% of CeA) [17] and CeO_2 (53% of CeA), which are in agreement with the calculated weight-loss values of 97%, 92%, 63% and 50%; the endothermic peak of 158 °C and the exothermic peaks of 201 °C and 250 °C shown in the DTA data suggest dehydration and the formation of cerium complexes of oxyacetate ($Ce(OH)(CH_3COO)$) and dioxocarbonate ($Ce_2O_2CO_3$) [17,18], respectively. For CeN, TGA shows that only two weight-loss stages of ~50 to ~230 °C and ~230 to ~800 °C are associated with dehydration of CeN ($Ce(NO_3)_3$) and the formation of CeO_2 [19] as shown in Fig. 1(b). The DTA diagram shows that the first two endothermic peaks are attributed to dehydration of CeN and the last endothermic peak is attributed to the decomposition of $Ce(NO_3)_3$ to CeO_2; the experimental weight percentages of these two stages are 74% and 41%, which are close to the expected values of 75% and 43%. Finally, for CeAN, the two major stages of decomposition are related to

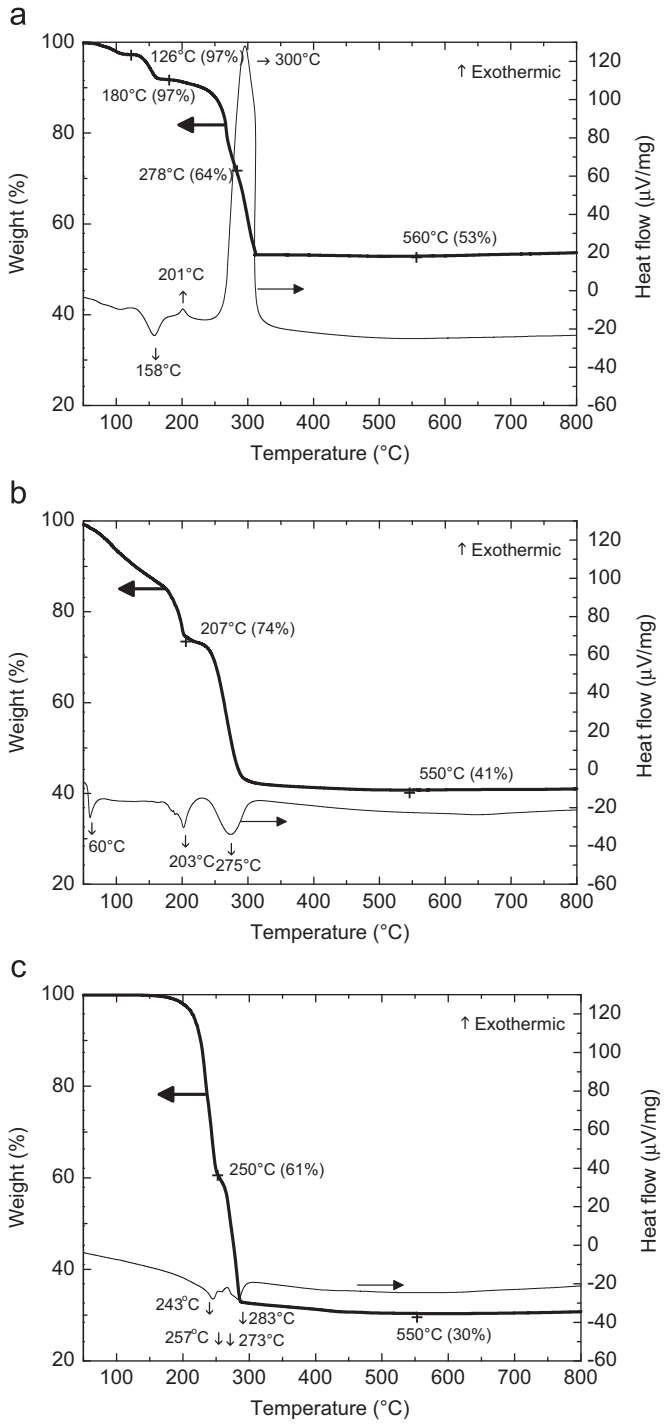

Fig. 1. The TGA and DTA data for the cerium salts of (a) CeA, (b) CeN and (c) CeAN.

the formation of $Ce(NO_3)_4$ (61% of CeAN) and CeO_2 (30% of CeAN) at the temperature ranges of ~50 to ~250 °C and ~250 to ~800 °C, respectively, as shown in Fig. 1(c). There are four endothermic peaks from 240 °C to ~280 °C associated with the transformation from CeAN to $Ce(NO_3)_4$ [20]. Overall, our results show that the remaining weight percentages of the three single salt systems (53% for CeA, 41% for CeN and 30% for CeAN) are in excellent agreement with the expected values (50% for CeA, 43% for CeN and 29% for CeAN).

Our previous study [11] has shown that four types of ceria particle morphologies can be controlled using the single salts CeA, CeN and CeAN: Types I (solid), II (hollow) and III

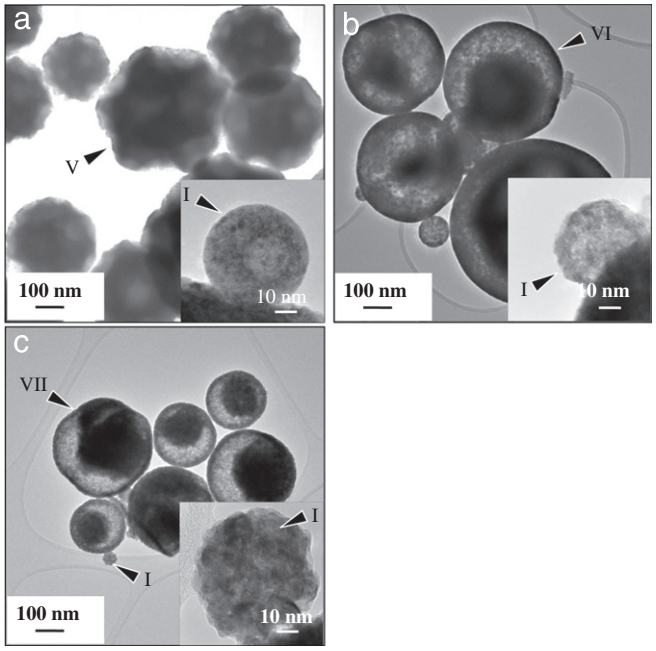

Fig. 2. The TEM images of the ceria particles prepared from the precursors of (a) CeA+CeN, (b) CeA+CeAN and (c) CeN+CeAN. High resolution images of a ceria particle are shown in the down-right corners of (a), (b) and (c), respectively. The various morphological types have been highlighted by triangles.

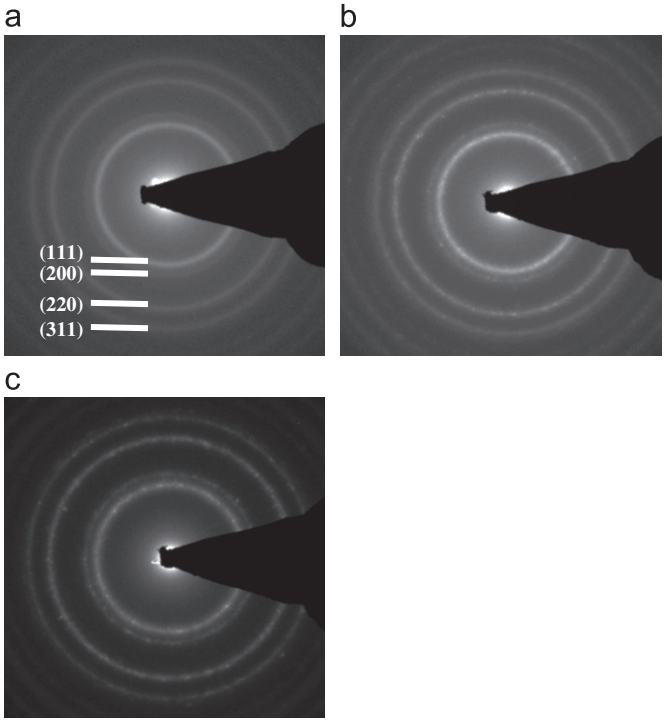

Fig. 3. The SAED patterns of the ceria particles prepared from the precursors of (a) CeA+CeN, (b) CeA+CeAN and (c) CeN+CeAN.

(concave) can be achieved using CeA; Types I, III and IV (porous) using CeN and Type I using CeAN. Fig. 2 shows the particle morphologies synthesized from the precursors complexes CeA+CeN, CeA+CeAN and CeN+CeAN. It can be seen that the morphologies resulting from the precursors of CeA+CeN (Fig. 2(a)) are Type I and a new crater-like morphology (Type V), the latter consisting of many concave surfaces. For CeA+CeAN (Fig. 2(b)), Type I and core–shell (Type VI) morphologies are observed, whereas for CeN+CeAN (Fig. 2(c)), Type I and macroporous (Type VII) are found. Fig. 3 shows SAED patterns from ceria particles synthesized from the above-mentioned three complexes. These patterns suggest that the particles consisted of randomly-orientated crystallites of the CeO_2 crystalline phase.

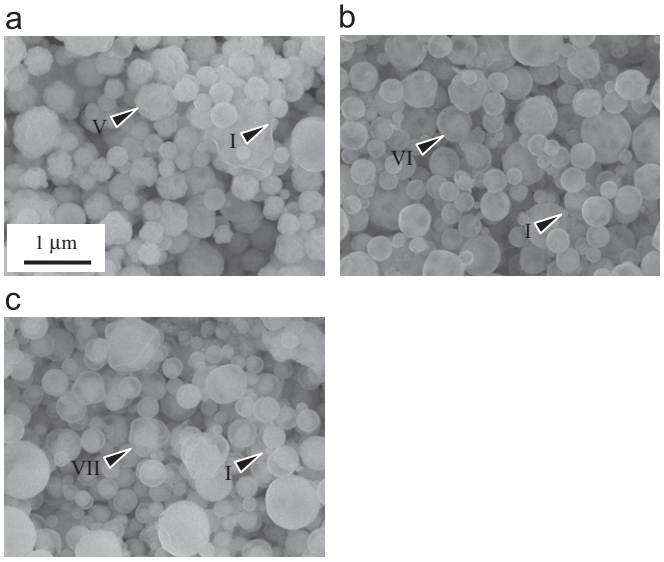

Fig. 4. The SEM images of the cerium particles prepared from the precursors of (a) CeA+CeN, (b) CeA+CeAN and (c) CeN+CeAN. The various morphological types have been highlighted by triangles.

The nature of the pores in the ceria particles has been characterized using a combination of TEM and SEM. As conventional TEM only characterizes the pores in term of two-dimensional projections; it is difficult to determine if the pores are open or closed [13]. In order to solve this problem, TEM results have been combined with SEM images to determine the pore's three-dimensional morphologies. Fig. 4 shows SEM images of the ceria particles obtained from the three precursor complexes. Fig. 4(a) and the TEM images in Fig. 2(a), Type V particles have been identified to possess shallow open pores (less than 100 nm in diameter). Fig. 4(b) together with Fig. 2(b) reveals that Type VI particles contain mostly closed pores. As shown in

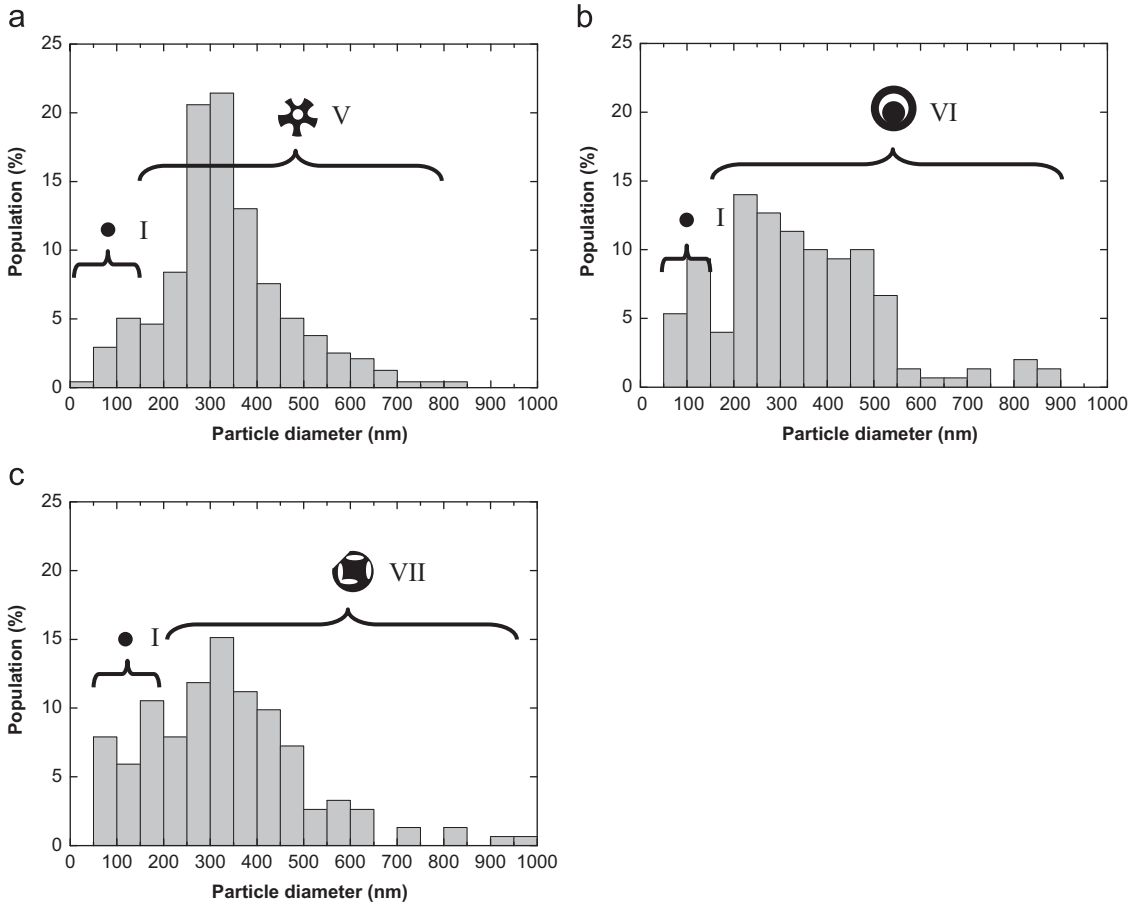

Fig. 5. Particle diameter histogram of ceria particles prepared from the precursors of (a) CeA+CeN, (b) CeA+CeAN and (c) CeN+CeAN. Schematic geometries related to different particle diameters are shown on the top of the corresponding size ranges.

Fig. 4(c), Type VII particles contain several deep, open pores (larger than 200 nm in diameter).

Fig. 5 shows the particle diameter distributions of ceria powders obtained from the three precursor complexes. The average particle diameters and the standard deviations obtained from the precursor complexes of CeA+CeN, CeA+CeAN and CeN+CeAN are 331 ± 135, 340 ± 171 and 340 ± 181 nm, respectively. The results indicate a similar average particle size in the three powders. The reason for such behavior is that the main factors controlling particle size, namely the precursor concentration and the ultrasonic frequency [21], were kept constant in this study. However, further examination of the detailed particle size distributions (Figs. 2 and 4) shows a correlation with their morphology. For CeA+CeN, the average diameters and standard deviations for Types I and V correspond to values 111 ± 58 and 345 ± 125 nm respectively; for CeA+CeAN, Types I and VI correspond to values of 138 ± 58 and 356 ± 162 nm respectively; for CeN+CeAN, Type I and Type VII correspond to values of 106 ± 111 and 379 ± 165 nm respectively. Among the three ceria powders, the averaged diameters of Type I particles are approximately 110 nm (111 nm for CeA+CeN, 138 nm for CeA+CeAN and 106 nm for CeN+CeAN), which are smaller than the other three particles morphologies (345 nm of Type V for CeA+CeN, 356 nm of Type VI for CeA+CeAN and 379 nm of Type VII for CeN+CeAN). These results reveal that the particle morphology is a function of the particle size. In addition, the surface areas of particles obtained from CeA+CeN, CeA+CeAN and CeN+CeAN are 3.7 ± 0.1 m^2/g, 7.3 ± 0.1 m^2/g and 32.1 ± 0.3 m^2/g, respectively.

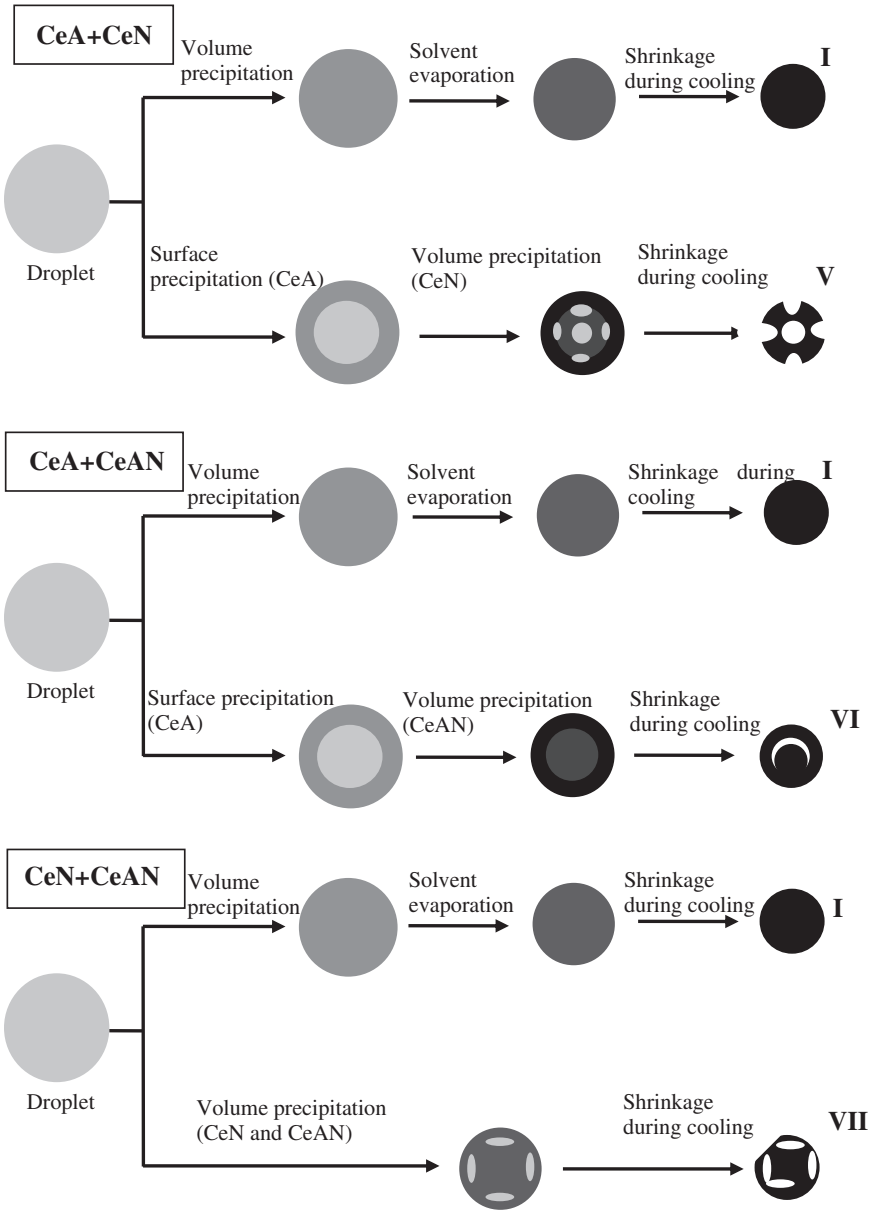

Fig. 6. Schematic diagram illustrating the formation mechanism of the main particle morphologies from the precursors of CeA+CeN, CeA+CeAN and CeN+CeAN for the SP stages.

Across the three ceria powders, the averaged diameters of Type I are similar, while the different values of surface area come from Types V, VI and VII, which implies Type VII particles (macroporous) have larger surface area than Type VI (core–shell) and Type V (crater-like) particles. Thus, the experimental result suggests that particle morphologies are controlled by the particle diameter and precursor complexes.

The precursor solutions undergo four stages of atomization, solvent evaporation, solute decomposition and particle sintering to form particles, as proposed by Messing et al. [16]. Fig. 6 shows a schematic diagram of the morphology formation mechanisms from the three precursor complexes for the SP stages. In the SP process, the factors influencing the particle morphology are suggested to be the solubility of the precursors, solvent evaporation rates and the melting temperature of the salt [13,22–24]. Firstly, the three precursors show two types of solubility behaviors. The solubility of CeA decrease with increasing temperature from 115 g/L at 15 °C to 100 g/L at 25 °C [25], whereas the solubilities of CeN and CeAN increase with increasing temperature from 637 g/L at 25 °C to 739 g/L at 50 °C [26] for CeN and from 1409 g/L at 25 °C to 2268 g/L at 85.6 °C [27] for CeAN. In addition, the melting temperatures of cerium nitrate hydrate, cerium ammonium nitrate and cerium acetate hydrate are 60 °C [19], 108 °C [28] and 300 °C [14], respectively. Due to the high solubility of CeAN and CeN salts, they should undergo volume precipitation to generate solid particles [16]. Although CeAN salts form solid particles, this is not the case for CeN salts (which from a porous structure). The main reason is that melting temperature of CeN (60 °C) is lower than that boiling temperature of water (100 °C), and the melting salts inhibit the removal of the entrapped water for the porous structure during heating [11]. However, the melting temperature of CeAN (300 °C) is higher than the temperature of boiling water, which does not inhibit the water removal to form a solid structure. According to solvent evaporation rates, volume and surface precipitation control the precursor droplets to form solid and hollow particles, respectively [16,24]. Initially, the solutes of the small droplets precipitate simultaneously in all volume (volume precipitation) to from solid particles (Type I). Due to the constancy of the ultrasonic frequency, the three precursor complexes all give rise to smaller Type I particles (~120 nm in diameter). In addition to the formation mechanism of Type I particles explained above, the details of formation mechanisms of the three other morphologies are given below. For Type V particles (from CeA+CeN), CeA salts precipitate first in a droplet surface to form a shell structure (surface precipitation) at ~85 °C where CeN salts still dissolve in water [13]. With increasing temperature, within the droplet, CeN salts form several pores (lower melting temperature) during the stages of solvent evaporation and solute decomposition [13]. At the cooling stage, the particles shrink with decreasing temperature to form several concaves on the particle surface, therefore giving the crater-like morphology. For CeA+CeAN, initially CeA salts form shell structures (surface precipitation). With increasing temperature, CeAN salts form solid spheres (volume precipitation) inside the shells [11] to form Type VI core–shell particles. Finally, for CeN+CeAN, in the droplet, the CeN and CeAN salts form porous and solid structures via volume precipitation, respectively, leading to Type VII particles with macroporous structures. Based on these experimental results, we have established the morphology formation mechanisms of various precursor complexes through their solubilities, solvent evaporation rates and melting temperatures.

4. Conclusions

Ceria particles of four main morphologies, namely: solid, crater-like, core–shell and macroporous have been obtained using the precursor complexes of CeA+CeN, CeA+CeAN and CeN+CeAN. The formation mechanisms of these morphologies have been explained based on the precursor solubilities, solvent evaporation rates and precursor melting temperatures. Our results show that these complex morphologies can be controlled for various applications by selecting suitable precursor complexes.

Acknowledgments

This work was funded by the National Science Council of Taiwan (Grant no. NSC 99-2218-E-011-030-MY2) and by the National Taiwan University of Science and Technology (Grant no. 100H451201).

References

[1] N.Q. Minh, Ceramic fuel-cells, Journal of the American Ceramic Society 76 (1993) 563–588.
[2] R.N. Blumenth, F.S. Brugner, J.E. Garnier, Electrical conductivity of CaO-doped nonstoichiometric cerium dioxide from 700 °C to 1500 °C, Journal of the Electrochemical Society 120 (1973) 1230–1237.
[3] G.Z. Chen, F.F. Zhu, X. Sun, S.X. Sun, R.P. Chen, Benign synthesis of ceria hollow nanocrystals by a template-free method, Crystal Engineering Communications 13 (2011) 2904–2908.
[4] U. Hennings, R. Reimert, Investigation of the structure and the redox behavior of gadolinium doped ceria to select a suitable composition for use as catalyst support in the steam reforming of natural gas, Applied Catalysis A—General 325 (2007) 41–49.
[5] X.J. Du, D.S. Zhang, L.Y. Shi, R.H. Gao, J.P. Zhang, Morphology dependence of catalytic properties of Ni/CeO_2 nanostructures for carbon dioxide reforming of methane, Journal of Physical Chemistry C 116 (2012) 10009–10016.
[6] N. Phonthammachai, M. Rumruangwong, E. Gulari, A.M. Jamieson, S. Jitkarnka, S. Wongkasemjit, Synthesis and rheological properties of mesoporous nanocrystalline CeO_2 via sol–gel process, Colloids and Surfaces A 247 (2004) 61–68.
[7] Y.L. Kuo, Y.M. Su, Sintering behaviour and electrical properties of gadolinia-doped ceria modified by addition of silicon oxide and titanium oxide, Micro and Nano Letters 7 (2012) 472–475.
[8] T. Masui, K. Fujiwara, K. Machida, G. Adachi, T. Sakata, H. Mori, Characterization of cerium(IV) oxide ultrafine particles prepared using reversed micelles, Chemistry of Materials 9 (1997) 2197–2204.
[9] A.S. Reddy, C.Y. Chen, C.C. Chen, S.H. Chien, C.J. Lin, K.H. Lin, C.L. Chen, S.C. Chang, Synthesis and characterization of Fe/CeO_2 catalysts: epoxidation of cyclohexene, Journal of Molecular Catalysis A—Chemical 318 (2010) 60–67.

[10] S.Y. Chen, C.H. Tsai, M.Z. Huang, D.C. Yan, T.W. Huang, A. Gloter, C.L. Chen, H.J. Lin, C.T. Chen, C.L. Dong, Concentration dependence of oxygen vacancy on the magnetism of CeO_2 nanoparticles, Journal of Physical Chemistry C 116 (2012) 8707–8713.
[11] S.J. Shih, Y.Y. Wu, C.Y. Chen, C.Y. Yu, Morphology and formation mechanism of ceria nanoparticles by spray pyrolysis, Journal of Nanoparticle Research 14 (2012) 1–9.
[12] H.S. Kang, Y.C. Kang, H.Y. Koo, S.H. Ju, D.Y. Kim, S.K. Hong, J.R. Sohn, K.Y. Jung, S.B. Park, Nano-sized ceria particles prepared by spray pyrolysis using polymeric precursor solution, Materials Science and Engineering B—Solid 127 (2006) 99–104.
[13] S.J. Shih, P.R. Herrero, G. Li, C.Y. Chen, S. Lozano-Perez, Three-dimensional structures of mesoporous ceria particles using electron tomography, Microscopy and Microanalysis 17 (2011) 54–60.
[14] C.Y. Chen, T.K. Tseng, C.Y. Tsay, C.K. Lin, Formation of irregular nanocrystalline CeO_2 particles from acetate-based precursor via spray pyrolysis, Journal of Materials Engineering and Performance 17 (2008) 20–24.
[15] S.J. Shih, K.B. Borisenko, L.J. Liu, C.Y. Chen, Multiporous ceria nanoparticles prepared by spray pyrolysis, Journal of Nanoparticle Research 12 (2010) 1553–1559.
[16] G.L. Messing, S.C. Zhang, G.V. Jayanthi, Ceramic powder synthesis by spray-pyrolysis, Journal of the American Ceramic Society 76 (1993) 2707–2726.
[17] A.I.Y. Tok, F.Y.C. Boey, Z. Dong, X.L. Sun, Hydrothermal synthesis of CeO_2 nano-particles, Journal of Materials Processing Technology 190 (2007) 217–222.
[18] M.J. Fuller, J. Pinkstone, Thermal analysis of the oxalate hexahydrates and decahydrates of yttrium and the lanthanide elements, Journal of Less-Common Metals 70 (1980) 127–142.
[19] E. Papastergiades, S. Argyropoulos, N. Rigakis, N.E. Kiratzis, Fabrication of ceramic electrolytic films by the method of solution aerosol thermolysis (SAT) for solid oxide fuel cells (SOFC), Ionics 15 (2009) 545–554.
[20] F. Bondioli, A.B. Corradi, C. Leonelli, T. Manfredini, Nanosized CeO_2 powders obtained by flux method, Materials Research Bulletin 34 (1999) 2159–2166.
[21] Y.L. Song, S.C. Tsai, C.Y. Chen, T.K. Tseng, C.S. Tsai, J.W. Chen, Y.D. Yao, Ultrasonic spray pyrolysis for synthesis of spherical zirconia particles, Journal of the American Ceramic Society 87 (2004) 1864–1871.
[22] S.J. Shih, L.Y.S. Chang, C.Y. Chen, K.B. Borisenko, D.J.H. Cockayne, Nanoscale yttrium distribution in yttrium-doped ceria powder, Journal of Nanoparticle Research 11 (2009) 2145–2152.
[23] S.J. Shih, G. Li, D.J.H. Cockayne, K.B. Borisenko, Mechanism of dopant distribution: an example of nickel-doped ceria nanoparticles, Scripta Materialia 61 (2009) 832–835.
[24] S.J. Shih, Y.Y. Wu, K.B. Borisenko, Control of morphology and dopant distribution in yttrium-doped ceria nanoparticles, Journal of Nanoparticle Research 13 (2011) 7021–7028.
[25] B.T. Kilbourn, Part 1, A–L, in: A Lanthanide Lantology, Molycorp Inc., Mountain Pass, 1993, 4 pp.
[26] L.L. Quill, R.F. Robey, The rare earth metals and their compounds. III. The ternary systems cerium group nitrates–nitric acid–water at 25 and 50°, Journal of the American Chemical Society 59 (1937) 2591–2595.
[27] A. Seidell, Solubilities of Inorganic and Organic Substances, D. Van Nostrand Company, New York, USA, 1919.
[28] N. Audebrand, N. Guillou, J.P. Auffrédic, D. Louë]r, The thermal behavior of ceric ammonium nitrate studied by temperature-dependent X-ray powder diffraction, Themochimica Acta 286 (1996) 83–87.